https://doi.org/10.5194/egusphere-2025-2808
Preprint. Discussion started: 28 July 2025
© Author(s) 2025. CC BY 4.0 License.

Analysis of a saline dust storm from the Aralkum Desert - Part 2: Atmospheric flow precursors in the Euro-Atlantic region

Xin Xi

Department of Geological and Mining Engineering and Sciences, Michigan Technological University, Houghton, MI, USA

Correspondence: Xin Xi (xinxi@mtu.edu)

Abstract.

Wind-blown dust emissions from the man-made Aralkum Desert pose significant environment and human health risks across Central Asia. Yet, little is known about the atmospheric circulation patterns favoring dust outbreaks from the region. This study examines the role of upstream atmospheric blocking and recurrent transient Rossby wave packets (RWPs) in initiating a severe dust storm from the Aralkum Desert in May 2018. Results show that the dust event was triggered by an unusual early-summer cold air outbreak and attendant postfrontal northerly winds reaching 24–31 m/s. The compound cold air and dust outbreaks were preceded by repeated meridional flow amplification linked to recurrent RWPs across the North Atlantic, persistent blocking over Scandinavia, and the subsequent development of a pronounced ridge-trough couplet that facilitated cold intrusions into Kazakhstan. This study underscores the importance of Euro-Atlantic blocking systems in shaping surface weather hazards in the downstream Central Asia region.

1 Introduction

Aral Sea was a shallow, brackish terminal lake situated within the Turanian basin of Central Asia, originally covering an area of 68,000 km^2, with an average depth of 16 m and a salinity of 10 g L^{-1} (Breckle and Geldyeva, 2012). The lake's water level was primarily sustained by inflows from the Amu Darya and Syr Darya rivers until the 1960s, when both rivers were excessively diverted to support large-scale irrigation for cotton and grain cultivation (Saiko and Zonn, 2000). Between 1960 and 2010, the area of irrigated lands in Central Asia nearly doubled, expanding from 4.5 to 8.2 million ha, leading to significant evaporation losses and reduced river discharges (Micklin, 2014). As a result, Aral Sea experienced rapid desiccation over the subsequent decades, as shown in Fig. 1. By the late 1980s, it had split into two main water bodies: the smaller North Aral Sea and the larger South Aral Sea, connected by the Berg Strait. In 2005, the construction of the Kokaral Dam effectively stopped the outflow from the North into South Aral, leading to partial restoration of the North Aral, as evidenced by the decreasing distance between the shoreline and the former fishing port of Aralsk, Kazakhstan (Fig. 1). In contrast, the South Aral Sea continued to shrink, eventually fragmenting into three remnant brine lakes: the deeper western basin, the shallow eastern basin, and Tsche-Bas Bay. By 2012, the Aral Sea had lost approximately 85% of its original surface area (Micklin, 2014). In 2014, the eastern basin dried up completely for the first time in modern history, likely due to a severe drought during the preceding year (Barlow and Hoell, 2015).

https://doi.org/10.5194/egusphere-2025-2808
Preprint. Discussion started: 28 July 2025
© Author(s) 2025. CC BY 4.0 License.

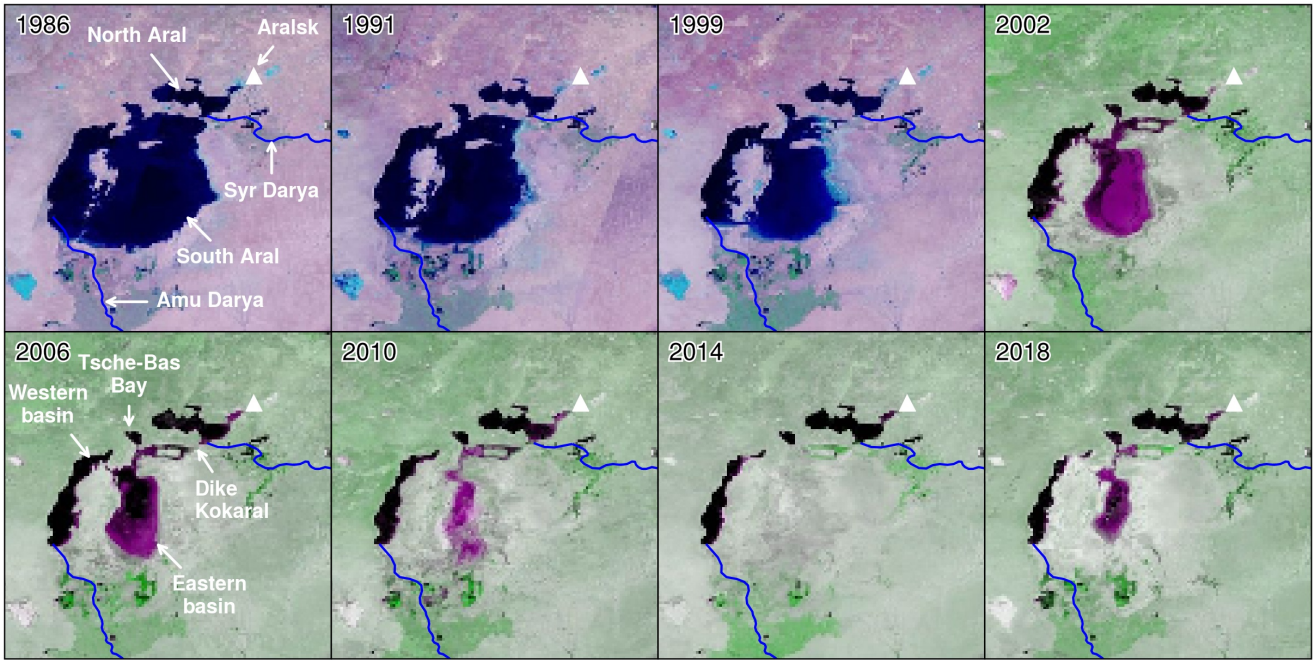

Figure 1. Desiccation of Aral Sea captured by Landsat (1986, 1991, 1999) and MODIS/Terra (2002 onward) satellites. The MODIS false color band combination (1-2-1) generates a pink appearance over the shallow eastern basin of South Aral. The city of Aralsk, Kazakhstan is indicated by a triangle.

Following the desiccation of the Aral Sea, a new desert, called Aralkum, emerged as a prominent regional hot spot for wind blown dust emissions (Xi and Sokolik, 2015, 2016). Ground observations revealed increasing dust frequency near Aralkum between the 1970s and 2000s, in contrast to declining trends over the rest of Central Asia (Indoitu et al., 2012). Early estimates suggested that Aralkum contributed approximately 7.3 Tg yr^{-1} dust emissions between 1966 and 1979 (Orlovsky and Orlovsky, 2001). More recently, Xi and Sokolik (2016) estimated that Aralkum emitted between 0.4 and 11.4 Tg yr^{-1} during 2000–2014, accounting for up to 14% of the total dust emissions in Central Asia. Similarly, Banks et al. (2022) estimated that Aralkum contributed 27 Tg or 14% to the regional dust emission in 2015, nearly doubling the emission from the 1980s.

Climatologically, Central Asia is prone to cold intrusions from late winter through early summer, which generate strong northerly and northwesterly winds capable of dust lifting from the region's dry, sparsely vegetated surfaces (Knippertz, 2014; Mohammadpour et al., 2022). It was estimated that more than 40% of the dust events in Central Asia are triggered by cold intrusions and their attendant sustained high winds (Orlovsky et al., 2005; Surkova, 2010). Smirnov et al. (1993) identified two primary types of dust-producing cold fronts in Central Asia: a shallow, density current-like front with minimal cloud development, and a deep cold front characterized by strong vertical development and distinct rearward-inclined cloud formation. More recently, (Xi et al., 2023) analyzed the meteorological dynamics of a record-breaking cold air and dust outbreak in Uzbekistan, and found that the compound weather hazard was facilitated by atmospheric blocking over western Siberia and the equatorward

https://doi.org/10.5194/egusphere-2025-2808
Preprint. Discussion started: 28 July 2025
© Author(s) 2025. CC BY 4.0 License.

displacement of a tropopause polar vortex. Atmospheric blocking is a long-lasting, quasi-stationary tropospheric flow pattern which blocks or decelerates the zonal westerly flow and induces large meridional flow components in the midlatitudes (Kautz et al., 2022). Blocking events preferably occur downstream of the Atlantic oceanic storm track, extending from eastern North Atlantic (especially Scandinavia) to western Siberia (near Ural Mountains). The persistent anticyclonic flow anomalies associated with blocking events provide extended periods for the formation and transport of cold airmasses towards the equator, such as Central Asia which is located downstream from European blocking systems (Tyrlis and Hoskins, 2008; Tuel and Martius, 2024).

On 27 May 2018, a severe dust storm was driven by cold air intrusion over the Aralkum Desert, causing record-high particulate matter concentrations, widespread haze, and salt deposition over agricultural lands. Xi (2023) hypothesized a possible link between the dust event and anomalous atmospheric circulation patterns in the Euro-Atlantic sector, but did not provide a formal analysis of the dynamic teleconnections involved. In the first part of a comprehensive investigation of the Aralkum dust storm, Xi et al. (2025) compared multiple satellite instruments and retrieval algorithms for aerosol column burden, vertical height, and particle properties, and found substantial inconsistencies and biases due to uncertainties in surface reflectances and aerosol microphysical properties. In this companion study, we investigate the large-scale atmospheric flow precursors of this dust event, particularly the role of atmospheric blocking and recurrent transient Rossby wave packets (RWPs) in the Euro-Atlantic sector.

2 Data and Methods

2.1 Identification of cold air and dust outbreaks

Surface synoptic observations (SYNOP) and ERA5 reanalysis data are used to evaluate the intensity and spatial extent of cold air and dust outbreaks during May 2018. SYNOP observations comprise 3-hourly weather station reports of temperature, sea level pressure (SLP), mean wind, maximum instantaneous wind speed, horizontal visibility, and present weather (ww) at various locations. The present weather codes, based on the FM-12 format, use numerical values to classify observed atmospheric conditions, such as haze (ww=5) and various dust-related phenomena (ww=6–9, 30–35) (Xi, 2021). Dusty days are identified as those with at least one report of dust-related weather, or a haze report following a dust weather report within the previous 48 hours. Cold anomaly days are defined as those when the daily mean temperature falls at least 1.5 standard deviations below the 1970–2018 climatological average for that calendar day. A cold air outbreak (CAO) is defined as a period of at least two consecutive cold anomaly days, similar to past studies (Vavrus et al., 2006; Wheeler et al., 2011). To further evaluate the severity of CAO events, we analyze the ERA5 daily mean 1000–500 hPa geopotential height thickness and calculate its percentile ranks relative to a 15-day climatological window centered on 27 May (i.e., 20 May–3 June) for the period 1960–2021. Percentile rank values close to zero indicate exceptionally cold air masses relative to the climatological distribution for that period.

https://doi.org/10.5194/egusphere-2025-2808
Preprint. Discussion started: 28 July 2025
© Author(s) 2025. CC BY 4.0 License.

2.2 Detection of upper tropospheric circulation anomalies

We use the ERA5 reanalysis to detect two types of upper-tropospheric flow anomalies that favor the development of extreme surface weather: atmospheric blocking and recurrent transient RWPs. Blocking is identified as regions with persistent (70% contour overlap between consecutive 6-hourly time steps for at least 5 days), negative anomalies of 150–500 hPa vertically averaged potential vorticity (PV) less than the 10th percentile of the daily climatological PV anomaly between 1959 and 2000 (Schwierz et al., 2004; Steinfeld, 2020; Tuel et al., 2022). Recurrent RWPs are identified based on the Hovmöller diagram of midlatitude upper-tropospheric meridional flows (Röthlisberger et al., 2019; Ali et al., 2021). Specifically, we first compute a 14-day running mean of the 250 hPa meridional winds, averaged over the 37°N–57°N latitude band. To isolate signals of synoptic-scale waves, we apply a Fourier decomposition and retain only wavenumbers in the range 4–15. A recurrence metric R is then calculated as the absolute magnitude of the time- and wavenumber-filtered signal. Large values of R indicate either persistent, quasi-stationary synoptic-scale waves or multiple transient wave packets moving in a recurrent manner such that the individual troughs and ridges repeatedly amplify at the same longitudes (Röthlisberger et al., 2019).

3 Results

3.1 Synoptic observations

Figure 2a exhibits the equatorward incursion of a large pool of cold airmass into Kazakhstan on 27 May 2018, with the daily mean 1000–500 hPa thickness falling below 540 dam, a typical value for distinguishing rain versus snow. Over the Aralkum Desert, the 1000–500 hPa thickness dropped below the 10th percentile relative to the 1960–2021 climatology, indicating an exceptionally cold airmass. This cold advection was facilitated by strong northerly winds along the eastern flank of a surface anticyclone centered over western Kazakhstan. SYNOP observations confirmed widespread cold anomalies on both 27 and 28 May, with the maximum instantaneous wind speed reaching 24–31 m s^{-1} near the Aralkum Desert.

On 27 May, strong postfrontal northerlies mobilized a broad, whitish dust plume from Aralkum, which swept across large parts of Uzbekistan and moved towards the Iran-Turkmenistan border, as observed by the Visible Infrared Imaging Radiometer Suite (VIIRS) aboard the NOAA-20 spacecraft (Fig. 2a). Xi et al. (2025) reported that the dust plume was so optically thick that satellite aerosol algorithms failed to retrieve its aerosol optical depth (AOD), with some retrievals even misclassifying the plume as clouds. On the next day, a surface anticyclone developed just south of the Aralkum Desert, redirecting the lofted dust westward toward the Caspian Sea (Fig. 2b). Xi et al. (2025) reported that the VIIRS-retrieved AOD reached the upper limit (5) in the algorithm, suggesting that the actual dust loading may have been even higher. Karami et al. (2021) found that the extreme AOD values observed during this event were significantly underestimated by aerosol models and reanalysis products. Local media reports suggested that particulate concentrations in the downwind Karakalpakstan and Khorezm regions exceeded the permissible levels by as much as sixfold (Gazeta, 2018). SYNOP observations from the city of Nukus, Karakalpakstan further reported visibility reductions to as low as 200 m due to the dust storm (Xi, 2023).

https://doi.org/10.5194/egusphere-2025-2808
Preprint. Discussion started: 28 July 2025
© Author(s) 2025. CC BY 4.0 License.

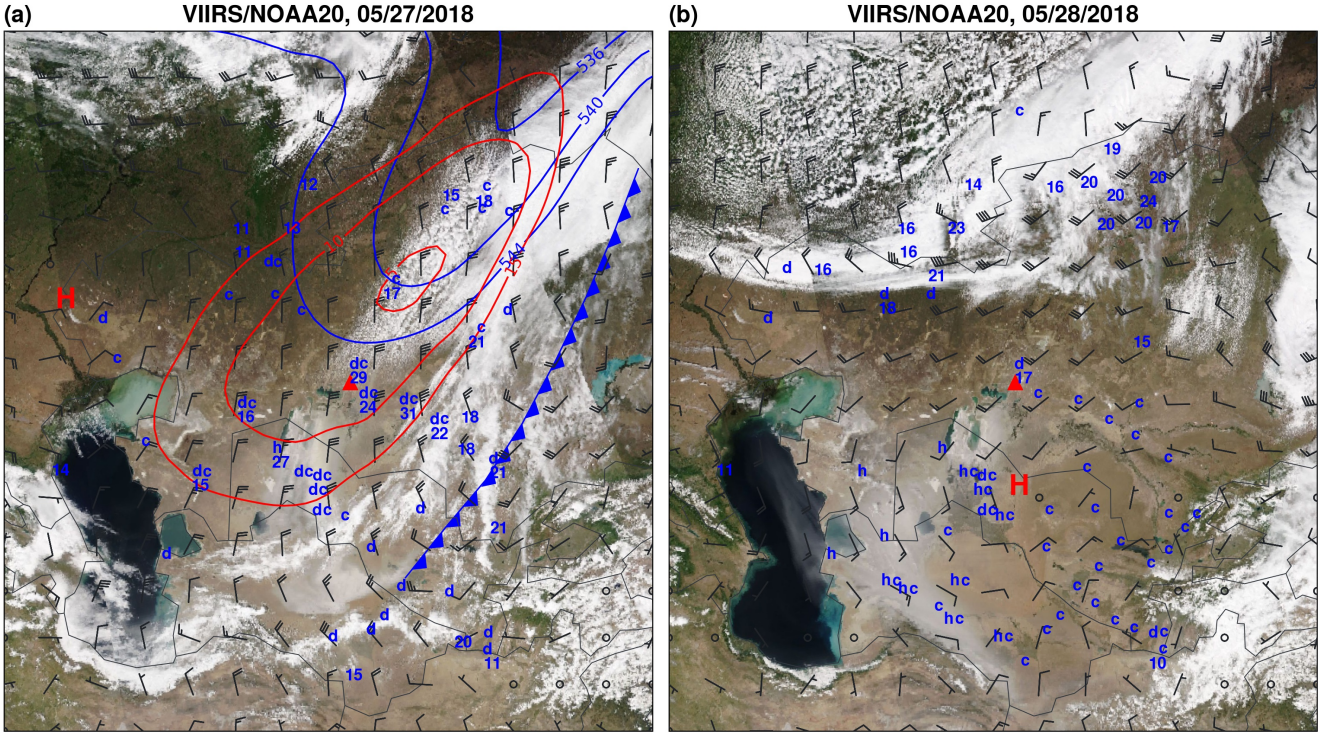

Figure 2. True color composites on 27 (a) and 28 (b) May 2018 from the Visible Infrared Imaging Radiometer Suite (VIIRS) instrument onboard the NOAA-20 spacecraft. The ERA5 925 hPa winds and surface synoptic observations (SYNOP) at 09 UTC are shown on both panels. The multi-parameter SYNOP reports are displayed as a combination of symbols: d for dust weather, h for haze weather, c for cold anomaly, numbers for maximum instantaneous wind speed. The contours in (a) indicate the daily mean 1000-500 hPa thickness (blue at 534, 540, and 546 dam) and corresponding percentile ranks within the 1960–2021 climatology (red at 5%, 10%, and 15%). The cold front, surface anticyclonic core (H), and Aralsk weather station (red triangle) are also indicated.

Figure 3a presents the 3-hourly SYNOP observations at Aralsk, Kazakhstan during 24–28 May 2018. As a former fishing port on the northern shore of Aral Sea (see Fig. 1), Aralsk provides long-term surface meteorological records representative of the Aralkum Desert. The Aralkum dust event was first reported at 15z 26 May and lasted for 24 hours. The event onset was accompanied with a sharp temperature drop of 12 °C, a pronounced reversal of SLP tendency from −11.6 to +20.5 hPa d^{-1},
105 and a shift in wind direction and intensity, with the instantaneous wind speeds reaching up to 29 m s^{-1}.

To evaluate how unusual these meteorological conditions were compared to past dust events recorded at Aralsk, we first identify all the dusty days between 1970 and 2021. For each of the dusty days, we compute the differences from the previous day in the daily mean, minimum, and maximum temperature and SLP, which serve as proxies for airmass changes and surface pressure gradients associated with the dust onset. In addition, the daily mean wind speed and dust uplift potential are calculated.
110 The dust uplift potential is defined as $u^3(1+u_t/u)(1-u_t^2/u^2)$ if $u > u_t$ else 0, where u is the wind speed and u_t= 6 m s^{-1} is the

https://doi.org/10.5194/egusphere-2025-2808
Preprint. Discussion started: 28 July 2025
© Author(s) 2025. CC BY 4.0 License.

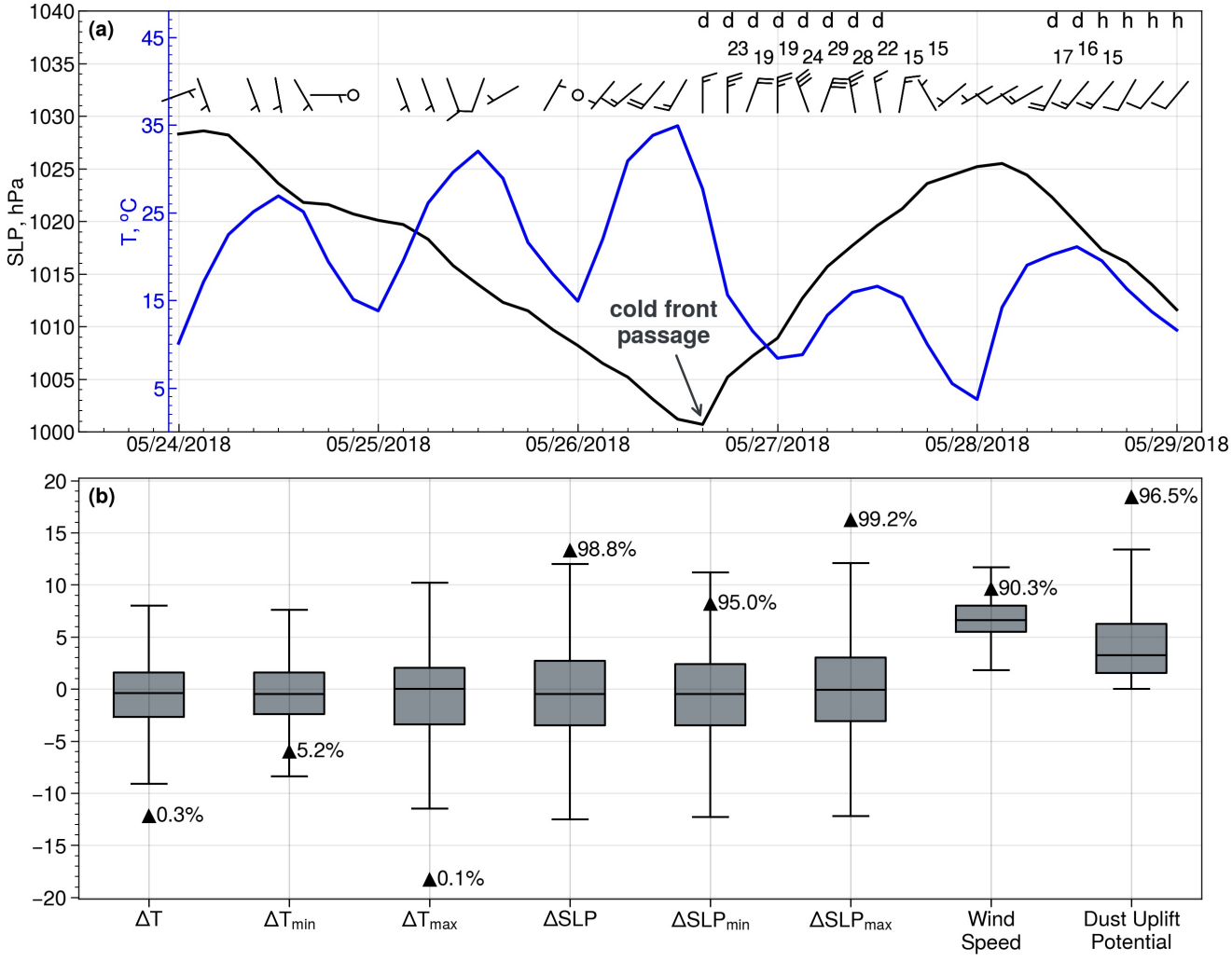

Figure 3. (a) 3-hourly surface synoptic observations at Aralsk, Kazakhstan. Dust and haze weather is marked as d and h, respectively. Numbers indicate the maximum instantaneous wind speed (misaligned for clarity). (b) Box plots for the observed meteorological indicators on all dusty days between 1970 and 2021, including differences from the previous day in the mean, minimum, and maximum temperature and SLP, mean wind speed, and dust uplift potential. The observed values on 27 May 2018 and associated percentile ranks are indicated as triangles.

https://doi.org/10.5194/egusphere-2025-2808
Preprint. Discussion started: 28 July 2025
© Author(s) 2025. CC BY 4.0 License.

threshold wind speed for dust emission (Cowie et al., 2015). Figure 3b displays the statistical distributions of these indicators, along with the observed values and their corresponding percentile ranks on 27 May 2018. The temperature and SLP indicators on this day reflect exceptionally strong cooling and rapid anticyclogenesis relative to the historical record. Specifically, the daily mean temperature dropped by −12 degrees from the previous day, which is ranked 0.3% among all the observed dusty days. The mean SLP rose by 13 hPa from the prior day, indicating extremely rapid pressure build-up (ranked 98%) over the Aralkum Desert. Furthermore, the observed wind speed and dust uplift potential indicate unusually intense winds and erosive power during the dust storm. Together, the SYNOP observations reveal record-strength CAO and high winds associated with the Aralkum dust storm.

3.2 Large-scale flow precursors

This section uses ERA5 reanalysis to investigate the large-scale atmospheric circulations leading up to the observed extreme surface weather. As shown in Fig. 4, a persistent blocking ridge (labeled as R1) was present over Scandinavia prior to the Aralkum dust storm. Although the blocking detection algorithm only identifies regions of negative PV anomaly (green contour) and excludes adjacent positive PV anomalies, the upper-tropospheric flow pattern exhibits a classic Omega block structure, characterized by a broad PV ridge over the eastern North Atlantic and Europe flanked by upstream and downstream PV troughs. Frequent wave breaking on the equatorward flank of the Atlantic jet stream, as indicated by the formation of stratospheric PV streamers and cut-off vortices, shifted the storm track northward and expanded the PV ridge westward, contributing to the persistence and reinforcement of the blocking regime (Hoskins et al., 1983; Masato et al., 2012). The persistent anticyclonic flow anomalies, which reportedly lasted from April to September, contributed to the early onset of record-breaking high temperatures across central and northern Europe, in association with enhanced large-scale subsidence and enhanced solar heating (Spensberger et al., 2020; Rousi et al., 2023). Contrary to the unusually dry hot summer over Europe, downstream regions of the Scandinavian block such as Central Asia are conducive to cold extremes or wintry conditions due to the equatorward transport of polar air masses (Konrad, 1998; Vavrus et al., 2006).

At 00z 25 May 2018, a pronounced PV gradient was observed upstream of a deep upper-level trough (T3) over the western subtropical Atlantic, coinciding with a strong, southwest-northeast oriented jet (Fig. 4a). At the left exit region of the jet, an extratropical cyclone (L) underwent rapid intensification, deepening from 987 to 976 hPa over the subsequent 12 hours (Fig. 4b). The extratropical cyclone features a coherent, poleward-ascending moist airstream from the subtropics, known as warm conveyor belt (WCB). The WCB outflow, characterized by strong mid-level ascent and upper-level divergence (Fig.4b), likely played an important role in the downstream flow amplification (Madonna et al., 2014; Pfahl et al., 2015; Steinfeld and Pfahl, 2019). Particularly, the jet stream accelerated and shifted poleward in the vicinity of the WCB outflow, fostering ridge amplification (R2) and blocking onset over the eastern North Atlantic. This amplifying ridge ultimately merged with the Scandinavian block (R1), reinforcing the large-scale quasi-stationary circulation pattern.

At the ground level, two intensifying anticyclones (H1 and H2) began to merge while slowly moving eastward. By 00z 26 May 2018, the Scandinavian block stretched into western Siberia and the Far North (Fig. 4c). Downstream of the block, positive PV advection led to the penetration of a PV trough (T1) into Kazakhstan (Fig. 4d), which explains the continuous SLP decrease

https://doi.org/10.5194/egusphere-2025-2808
Preprint. Discussion started: 28 July 2025
© Author(s) 2025. CC BY 4.0 License.

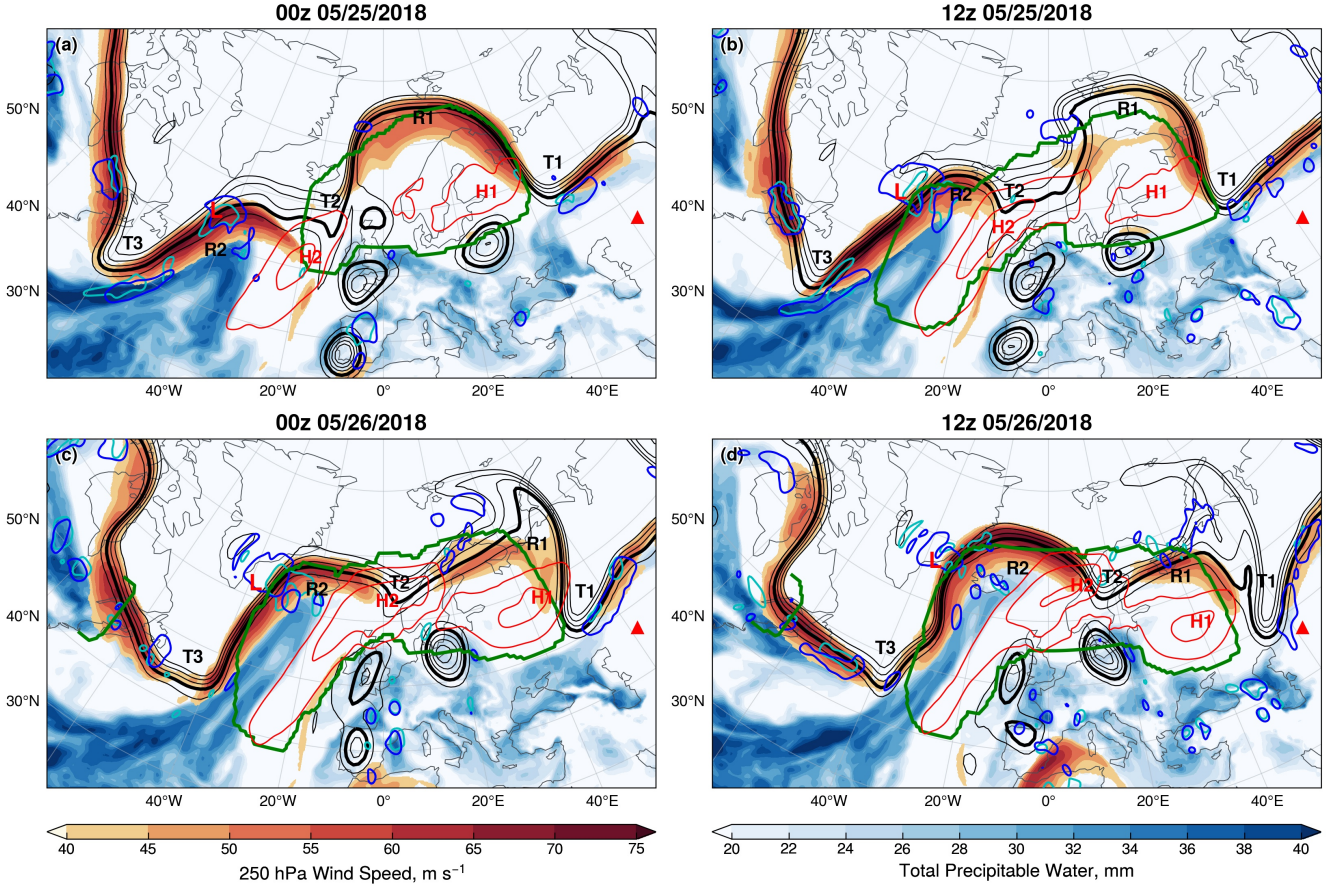

Figure 4. Large-scale atmospheric flow patterns over the Euro-Atlantic region at (a) 00z 25 May 2018, (b) 12z 25 May 2018, (c) 00z 26 May 2018, and (d) 12z 26 May 2018. Shown are the 320 K isentropic PV (black contours every 1 pvu starting at 1 pvu; 2 pvu in bold; 1 pvu=10^{-6} $Km^2s^{-1}kg^{-1}$), atmospheric blocking (green contours), 300–200 hPa averaged divergence (cyan contours at 2×10^{-5} s^{-1}), 600–400 hPa averaged vertical velocity (blue contours at −0.3 Pa s^{-1}), sea level pressure (red contours at 1028, 1032, and 1036 hPa), 250 hPa wind speed (red shading), and total precipitable water (blue shading). The extratropical cyclone (L), ridges (R1–R2), troughs (T1–T3), and surface anticyclones (H1–H2) are labeled. The city of Aralsk, Kazakhstan is denoted by a red triangle.

https://doi.org/10.5194/egusphere-2025-2808
Preprint. Discussion started: 28 July 2025
© Author(s) 2025. CC BY 4.0 License.

preceding the cold front passage (Fig. 3a). A cyclonic wave breaking event over the Barents Sea may have further contributed to the deepening and broadening of the PV trough, as well as the southward displacement of the jet. This ridge-trough couplet (R1 and T1) formed a distinctive upper-level flow configuration favoring deep meridional transport of polar airmasses into the midlatitudes (Colucci and Davenport, 1987; Konrad and Colucci, 1989; Konrad, 1996; Lupo et al., 2001).

The above analysis identifies atmospheric blocking over Scandinavia and western Siberia as a key precursor to the compound cold air and dust outbreaks over the Aralkum Desert in May 2018. There is also evidence that recurrent RWPs may have contributed to the stationary flow pattern, as seen in Fig. 4. Figure 5a reveals that a recurrent wave pattern emerged over the North Atlantic after mid-May 2018, when a succession of at least six transient RWPs propagated eastward in a similar phase with one another, resulting in persistently elevated R values between 60°W and 0°E. In particular, large R values were observed upstream of the Scandinavian block with a lead time of 2–3 days, suggesting that RWPs may have served as precursors to the blocking onset, possibly via Rossby wave breaking over the eastern North Atlantic (4), as suggested in previous studies Altenhoff et al. (2008); Röthlisberger et al. (2019). The RWP spanning 24–26 May 2018, with its individual ridges (R1, R2) and troughs (T1, T2, T3) depicted in Fig. 4 and 5a, was itself preceded by two earlier RWPs that initiated the recurrent wave pattern on 19 May 2018. At that time, the Aralkum Desert was situated underneath a broad blocking ridge. It was until 26 May that the deepening of an upper-level trough into Central Asia initiated a prolonged CAO event during 27–30 May and strong northerly winds sweeping across the Aralkum Desert.

Recurrent transient RWPs are also observed over the North Pacific throughout May 2018. At the end of the month, two long-lived RWPs contributed to an extensive area of elevated R values with co-located blocking over the North Atlantic. The recurrent and quasi-stationary (i.e., blocking) wave patterns caused a series of impactful weather conditions across the Northern Hemisphere during May 2018 (Fig. 5b), including above-normal temperatures over North America and East Asia, record-breaking warmth over central and northern Europe, and below-normal temperatures over northeastern Canada, western Russia, and Central Asia (NOAA, 2018; Kornhuber et al., 2019; Rösner et al., 2019; Sun et al., 2020). In addition, wave breaking and PV cut-offs downstream of the Scandinavian block led to frequent moist convection and flash floods in western Europe during the second half of May 2018 (Mohr et al., 2020). Persistent troughing south of Greenland facilitated enhanced poleward warm advection, potentially contributing to reduced Arctic sea ice extent (NOAA, 2018). Taken together, the cold air and dust outbreaks over the Aralkum Desert were part of spatially compounding climate anomalies and extremes, dynamically linked by recurrent and quasi-stationary wave patterns across the Northern Hemisphere.

4 Conclusions

This study examines the large-scale atmospheric flow precursors of a saline dust storm originating from the Aralkum Desert in May 2018. ERA5 reanalysis and surface synoptic observations indicate that the dust event was triggered by a severe cold air outbreak and attendant postfrontal northerly winds of 24–31 m s^{-1}. The compound cold air and dust outbreaks were supported by persistent atmospheric blocking over Scandinavia and intensification of an upper level trough into Kazakhstan. The Scandinavian block was facilitated by repeated meridional flow amplification associated with recurrent transient Rossby

https://doi.org/10.5194/egusphere-2025-2808
Preprint. Discussion started: 28 July 2025
© Author(s) 2025. CC BY 4.0 License.

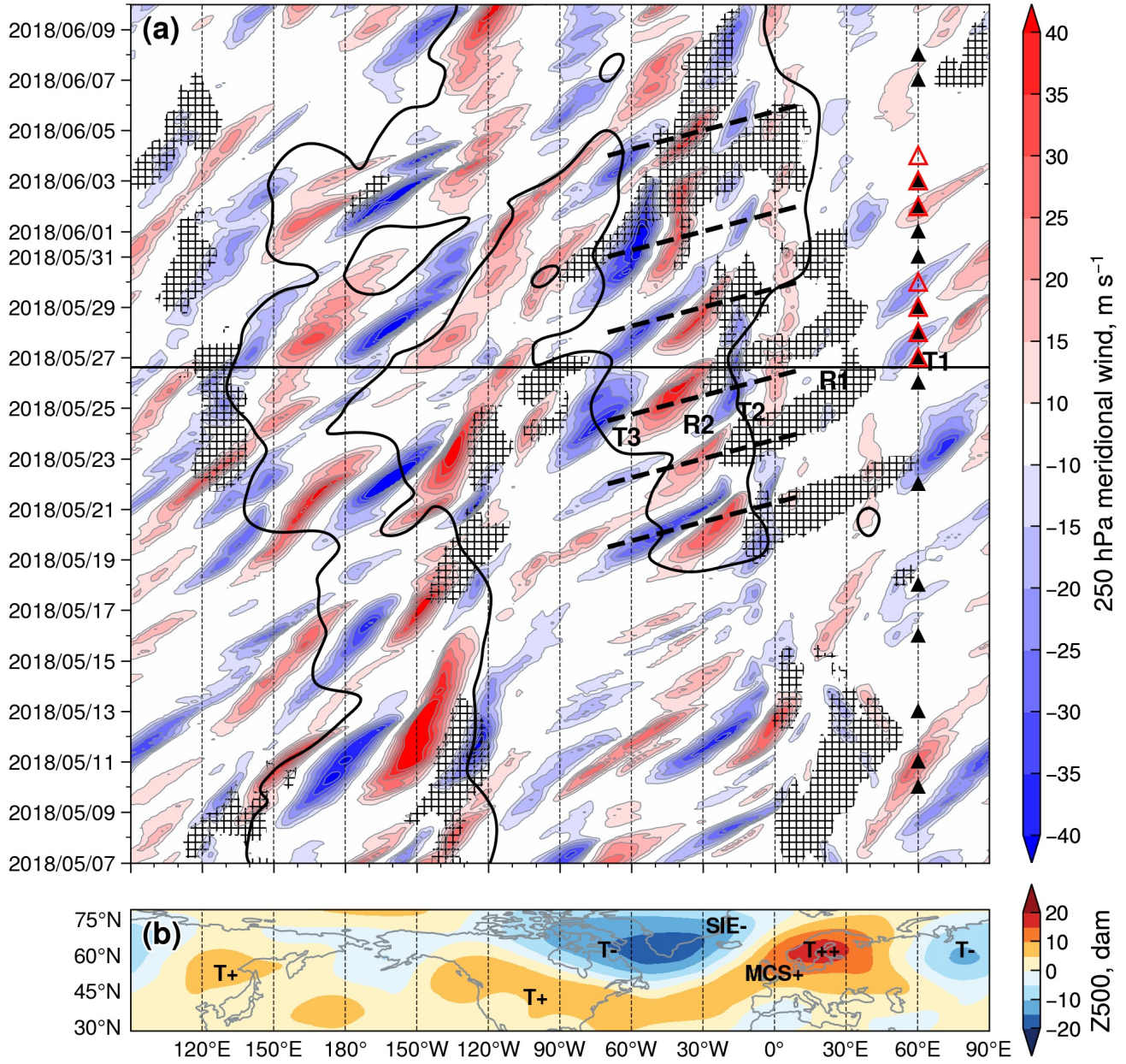

Figure 5. (a) Hovmöller diagram of 3-hourly 250 hPa, 37°N–57°N averaged meridional winds. Black contours indicate R metric values of 8 m s^{-1}. Hatched areas indicate longitudes at which at least half of grid points between 50°N–70°N feature an atmospheric block. Dashed lines indicate the longitude–time trajectories of six transient Rossby wave packets building up the recurrent wave pattern over the North Atlantic. Ridges and troughs of the Rossby wave packet leading to the dust storm are labeled as R1–R2 and T1–T3 (also shown in Fig. 4). The Aralkum dust storm onset is indicated by a horizontal line. Dusty and cold anomaly days at Aralsk, Kazakhstan are indicated as black solid and red open triangles, respectively. (b) 500 hPa geopotential height (Z500) anomaly in May 2018 relative to the climatological May average of 1961–2000. Reported climate anomalies and extremes in May 2018 include warmer-than-average (T+), record-breaking warmth (T++), colder-than-average (T−), above-average mesoscale convective system activity (MCS+), and below-average sea ice extent (SIE−).

https://doi.org/10.5194/egusphere-2025-2808
Preprint. Discussion started: 28 July 2025
© Author(s) 2025. CC BY 4.0 License.

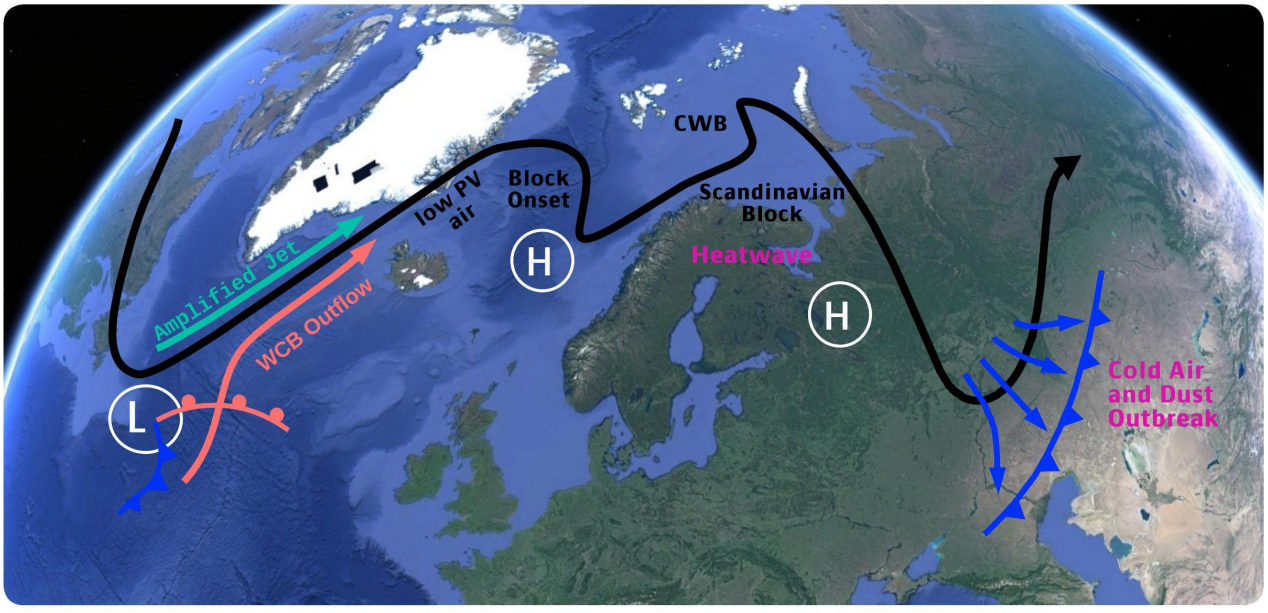

Figure 6. Schematic illustration of the large-scale atmospheric flow precursors of the compound cold air and dust outbreaks over the Aralkum Desert during May 2018. PV, Potential Vorticity. WCB, Warm Conveyor Belt. CWB, Cyclonic Wave Breaking.

wave packets across the North Atlantic. Diabatic processes within the poleward ascending airstreams of the transient waves likely played an important role in the upper-level flow amplification, wave breaking, and blocking maintenance. A schematic summary of the synoptic-dynamic processes is presented in Fig. 6.

The findings underscore the important role of large-scale teleconnections via recurrent and quasi-stationary wave patterns in driving the co-occurrence of cold air and dust outbreaks in Central Asia. However, the exact location of co-occurring cold spell and dust events depends on the amplitude and positioning of the blocking system relative to the dust-producing area. For example, the record-breaking dust storm in Uzbekistan in early November 2021 was linked to blocking over the Ural and West Siberia regions, which promoted the equatorward transport of a tropopause polar vortex into northeastern Kazakhstan (Xi et al., 2023). In comparison, the Aralkum dust storm examined in this study was associated with Scandinavian blocking and cold intrusion into western Kazakhstan. A deeper understanding of blocking dynamics in the Euro-Atlantic region may therefore improve the forecasting of compound cold air and dust outbreaks in Central Asia.

Data availability. ERA5 reanalysis product is available at https://doi.org/10.24381/cds.adbb2d47. Blocking and recurrent RWP detection results are available at https://doi.org/10.5281/zenodo.14027548.

https://doi.org/10.5194/egusphere-2025-2808
Preprint. Discussion started: 28 July 2025
© Author(s) 2025. CC BY 4.0 License.

Acknowledgements. This work is supported by the NASA Land Cover and Land Use Change (LCLUC) Program.

https://doi.org/10.5194/egusphere-2025-2808
Preprint. Discussion started: 28 July 2025
© Author(s) 2025. CC BY 4.0 License.

References

Ali, S. M., Martius, O., and Röthlisberger, M.: Recurrent Rossby Wave Packets Modulate the Persistence of Dry and Wet Spells Across the Globe, Geophysical Research Letters, 48, https://doi.org/10.1029/2020GL091452, 2021.

Altenhoff, A. M., Martius, O., Croci-maspoli, M., Schwierz, C., and Davies, H. C.: Linkage of atmospheric blocks and synoptic-scale Rossby waves: A climatological analysis, Tellus, Series A: Dynamic Meteorology and Oceanography, 60, 1053–1063, https://doi.org/10.1111/j.1600-0870.2008.00354.x, 2008.

Banks, J. R., Heinold, B., and Schepanski, K.: Impacts of the Desiccation of the Aral Sea on the Central Asian Dust Life-Cycle, Journal of Geophysical Research: Atmospheres, 127, https://doi.org/10.1029/2022JD036618, 2022.

Barlow, M. and Hoell, A.: Drought in the middle east and central-southwest Asia during winter 2013/14, Bulletin of the American Meteorological Society, 96, S71–S76, https://doi.org/10.1175/BAMS-D-15-00127.1, 2015.

Breckle, S.-W. and Geldyeva, G. V.: Dynamics of the Aral Sea in Geological and Historical Times, in: Aralkum - a Man-Made Desert: The Desiccated Floor of the Aral Sea (Central Asia), edited by Breckle, S.-W., Wucherer, W., Dimeyeva, L. A., and Ogar, N. P., pp. 13–35, Springer Berlin Heidelberg, Berlin, Heidelberg, ISBN 978-3-642-21117-1, https://doi.org/10.1007/978-3-642-21117-1_2, 2012.

Colucci, S. J. and Davenport, J. C.: Rapid surface anticyclogenesis: synoptic climatology and attendant large-scale circulation changes., Monthly Weather Review, 115, 822–836, https://doi.org/10.1175/1520-0493(1987)115<0822:RSASCA>2.0.CO;2, 1987.

Cowie, S. M., Marsham, J. H., and Knippertz, P.: The importance of rare, high-wind events for dust uplift in northern Africa, Geophysical Research Letters, 42, 8208–8215, https://doi.org/10.1002/2015GL065819, 2015.

Gazeta: The dust content in the air in the Aral Sea region exceeded the norm by almost 6 times, https://www.gazeta.uz/ru/2018/05/28/sand-salt/, 2018.

Hoskins, B. J., James, I. N., and White, G. H.: The shape, propagation and mean-flow interaction of large-scale weather systems., Journal of the Atmospheric Sciences, 40, 1595–1612, https://doi.org/10.1175/1520-0469(1983)040<1595:TSPAMF>2.0.CO;2, 1983.

Indoitu, R., Orlovsky, L., and Orlovsky, N.: Dust storms in Central Asia: Spatial and temporal variations, Journal of Arid Environments, 85, 62–70, https://doi.org/10.1016/j.jaridenv.2012.03.018, 2012.

Karami, S., Hossein Hamzeh, N., Kaskaoutis, D. G., Rashki, A., Alam, K., and Ranjbar, A.: Numerical simulations of dust storms originated from dried lakes in central and southwest Asia: The case of Aral Sea and Sistan Basin, Aeolian Research, 50, https://doi.org/10.1016/j.aeolia.2021.100679, 2021.

Kautz, L. A., Martius, O., Pfahl, S., Pinto, J. G., Ramos, A. M., Sousa, P. M., and Woollings, T.: Atmospheric blocking and weather extremes over the Euro-Atlantic sector - A review, Weather and Climate Dynamics, 3, 305–336, https://doi.org/10.5194/wcd-3-305-2022, 2022.

Knippertz, P.: Meteorological aspects of dust storms, in: Mineral Dust: A Key Player in the Earth System, pp. 121–147, Springer Dordrecht, ISBN 9789401789783, https://doi.org/10.1007/978-94-017-8978-3_6, 2014.

Konrad, C. E.: Relationships between the intensity of cold-air outbreaks and the evolution of synoptic and planetary-scale features over North America, Monthly Weather Review, 124, 1067–1083, https://doi.org/10.1175/1520-0493(1996)124<1067:RBTIOC>2.0.CO;2, 1996.

Konrad, C. E.: Persistent planeary scale circulation patterns and their relationship with cold air outbreak activity over the eastern United States, International Journal of Climatology, 18, 1209–1221, https://doi.org/10.1002/(SICI)1097-0088(199809)18:11<1209::AID-JOC301>3.0.CO;2-K, 1998.

Konrad, C. E. and Colucci, S. J.: An examination of extreme cold air outbreaks over eastern North America, Monthly Weather Review, 117, 2687–2700, https://doi.org/10.1175/1520-0493(1989)117<2687:AEOECA>2.0.CO;2, 1989.

https://doi.org/10.5194/egusphere-2025-2808
Preprint. Discussion started: 28 July 2025
© Author(s) 2025. CC BY 4.0 License.

Kornhuber, K., Osprey, S., Coumou, D., Petri, S., Petoukhov, V., Rahmstorf, S., and Gray, L.: Extreme weather events in early summer 2018 connected by a recurrent hemispheric wave-7 pattern, Environmental Research Letters, 14, https://doi.org/10.1088/1748-9326/ab13bf, 2019.

Lupo, A. R., Nocera, J. J., Bosart, L. F., Hoffman, E. G., and Knight, D. J.: South American cold surges: Types, composites, and case studies, Monthly Weather Review, 129, 1021–1041, https://doi.org/10.1175/1520-0493(2001)129<1021:SACSTC>2.0.CO;2, 2001.

Madonna, E., Wernli, H., Joos, H., and Martius, O.: Warm conveyor belts in the ERA-Interim Dataset (1979-2010). Part I: Climatology and potential vorticity evolution, Journal of Climate, 27, 3–26, https://doi.org/10.1175/JCLI-D-12-00720.1, 2014.

Masato, G., Hoskins, B. J., and Woollings, T. J.: Wave-breaking characteristics of midlatitude blocking, Quarterly Journal of the Royal Meteorological Society, 138, 1285–1296, https://doi.org/10.1002/qj.990, 2012.

Micklin, P.: Introduction to the Aral Sea and Its Region, in: The Aral Sea: The Devastation and Partial Rehabilitation of a Great Lake, edited by Micklin, P., Aladin, N., and Plotnikov, I., chap. 2, pp. 15–40, Springer Berlin Heidelberg, Berlin, Heidelberg, ISBN 978-3-642-02356-9, https://doi.org/10.1007/978-3-642-02356-9_2, 2014.

Mohammadpour, K., Sciortino, M., Kaskaoutis, D. G., and Rashki, A.: Classification of synoptic weather clusters associated with dust accumulation over southeastern areas of the Caspian Sea (Northeast Iran and Karakum desert), Aeolian Research, 54, https://doi.org/10.1016/j.aeolia.2022.100771, 2022.

Mohr, S., Wilhelm, J., Wandel, J., Kunz, M., Portmann, R., Punge, H. J., Schmidberger, M., Quinting, J. F., and Grams, C. M.: The role of large-scale dynamics in an exceptional sequence of severe thunderstorms in Europe May–June 2018, Weather and Climate Dynamics, 1, 325–348, https://doi.org/10.5194/wcd-1-325-2020, 2020.

NOAA: Monthly Global Climate Report for May 2018, published online June 2018, retrieved on May 19 2024, https://www.ncei.noaa.gov/access/monitoring/monthly-report/global/201805, 2018.

Orlovsky, L. and Orlovsky, N.: White sand storms in Central Asia, in: Global Alarm: Dust and Sand Storms from the World's Dry lands, edited by Yang, Y., Squires, V., and Lu, Q., chap. 8, pp. 169–201, United Nations, 2001.

Orlovsky, L., Orlovsky, N., and Durdyev, A.: Dust storms in Turkmenistan, Journal of Arid Environments, 60, 83–97, https://doi.org/10.1016/j.jaridenv.2004.02.008, 2005.

Pfahl, S., Schwierz, C., Croci-Maspoli, M., Grams, C. M., and Wernli, H.: Importance of latent heat release in ascending air streams for atmospheric blocking, Nature Geoscience, 8, 610–614, https://doi.org/10.1038/ngeo2487, 2015.

Rösner, B., Benedict, I., Heerwaarden, C. v., Weerts, A., Hazeleger, W., Bissolli, P., and Trachte, K.: Sidebar 7.3: The long heat wave and drought in Europe in 2018, in: State of the Climate in 2018, edited by Blunden, J. & Arndt, D. S., vol. 100, pp. S222–S223, Bulletin of the American Meteorological Society, https://doi.org/10.1175/2019BAMSStateoftheClimate.1, 2019.

Röthlisberger, M., Frossard, L., Bosart, L. F., Keyser, D., and Martius, O.: Recurrent synoptic-scale Rossby wave patterns and their effect on the persistence of cold and hot spells, Journal of Climate, 32, 3207–3226, https://doi.org/10.1175/JCLI-D-18-0664.1, 2019.

Rousi, E., Fink, A. H., Andersen, L. S., Becker, F. N., Beobide-Arsuaga, G., Breil, M., Cozzi, G., Heinke, J., Jach, L., Niermann, D., Petrovic, D., Richling, A., Riebold, J., Steidl, S., Suarez-Gutierrez, L., Tradowsky, J. S., Coumou, D., Düsterhus, A., Ellsäßer, F., Fragkoulidis, G., Gliksman, D., Handorf, D., Haustein, K., Kornhuber, K., Kunstmann, H., Pinto, J. G., Warrach-Sagi, K., and Xoplaki, E.: The extremely hot and dry 2018 summer in central and northern Europe from a multi-faceted weather and climate perspective, Natural Hazards and Earth System Sciences, 23, 1699–1718, https://doi.org/10.5194/nhess-23-1699-2023, 2023.

Saiko, T. A. and Zonn, I. S.: Irrigation expansion and dynamics of desertification in the Circum-Aral region of Central Asia, Applied Geography, 20, 349–367, https://doi.org/10.1016/S0143-6228(00)00014-X, 2000.

https://doi.org/10.5194/egusphere-2025-2808
Preprint. Discussion started: 28 July 2025
© Author(s) 2025. CC BY 4.0 License.

Schwierz, C., Croci-Maspoli, M., and Davies, H. C.: Perspicacious indicators of atmospheric blocking, Geophysical Research Letters, 31, https://doi.org/10.1029/2003gl019341, 2004.

Smirnov, V. V., Johnson, T. C., Krapivtseva, G. M., Krivchikova, T. V., and Shukurov, A. H.: Synoptic meteorological conditions during the U.S.S.R./U.S. dust experiment in Tadzhikistan in September 1989, Atmospheric Environment Part A, General Topics, 27, 2471–2479, https://doi.org/10.1016/0960-1686(93)90018-T, 1993.

Spensberger, C., Madonna, E., Boettcher, M., Grams, C. M., Papritz, L., Quinting, J. F., Röthlisberger, M., Sprenger, M., and Zschenderlein, P.: Dynamics of concurrent and sequential Central European and Scandinavian heatwaves, Quarterly Journal of the Royal Meteorological Society, 146, 2998–3013, https://doi.org/10.1002/qj.3822, 2020.

Steinfeld, D.: ConTrack - Contour Tracking (https://github.com/steidani/ConTrack), https://github.com/steidani/ConTrack, 2020.

Steinfeld, D. and Pfahl, S.: The role of latent heating in atmospheric blocking dynamics: a global climatology, Climate Dynamics, 53, 6159–6180, https://doi.org/10.1007/s00382-019-04919-6, 2019.

Sun, Y., Dong, S., Hu, T., Zhang, X., and Stott, P.: Attribution of the warmest spring of 2018 in northeastern Asia using simulations of a coupled and an atmospheric model, Bulletin of the American Meteorological Society, 101, S129–S134, https://doi.org/10.1175/BAMS-D-19-0264.1, 2020.

Surkova, G. V.: Regional climate variability, in: Handbook of Environmental Chemistry, edited by Kostianoy, A. G. and Kosarev, A. N., vol. 7, pp. 83–100, Springer Berlin Heidelberg, Berlin, Heidelberg, ISBN 978-3-540-88277-0, https://doi.org/10.1007/698_2009_2, 2010.

Tuel, A. and Martius, O.: Persistent warm and cold spells in the Northern Hemisphere extratropics: regionalisation, synoptic-scale dynamics and temperature budget, Weather and Climate Dynamics, 5, 263–292, https://doi.org/10.5194/wcd-5-263-2024, 2024.

Tuel, A., Steinfeld, D., Ali, S. M., Sprenger, M., and Martius, O.: Large-Scale Drivers of Persistent Extreme Weather During Early Summer 2021 in Europe, Geophysical Research Letters, 49, https://doi.org/10.1029/2022GL099624, 2022.

Tyrlis, E. and Hoskins, B. J.: Aspects of a northern hemisphere atmospheric blocking climatology, Journal of the Atmospheric Sciences, 65, 1638–1652, https://doi.org/10.1175/2007JAS2337.1, 2008.

Vavrus, S., Walsh, J. E., Chapman, W. L., and Portis, D.: The behavior of extreme cold air outbreaks under greenhouse warming, International Journal of Climatology, 26, 1133–1147, https://doi.org/10.1002/joc.1301, 2006.

Wheeler, D. D., Harvey, V. L., Atkinson, D. E., Collins, R. L., and Mills, M. J.: A climatology of cold air outbreaks over North America: WACCM and ERA-40 comparison and analysis, Journal of Geophysical Research Atmospheres, 116, https://doi.org/10.1029/2011JD015711, 2011.

Xi, X.: Revisiting the Recent Dust Trends and Climate Drivers Using Horizontal Visibility and Present Weather Observations, Journal of Geophysical Research: Atmospheres, 126, https://doi.org/10.1029/2021JD034687, 2021.

Xi, X.: On the Geomorphic, Meteorological, and Hydroclimatic Drivers of the Unusual 2018 Early Summer Salt Dust Storms in Central Asia, Journal of Geophysical Research: Atmospheres, 128, https://doi.org/10.1029/2022JD038089, 2023.

Xi, X. and Sokolik, I. N.: Seasonal dynamics of threshold friction velocity and dust emission in Central Asia, Journal of Geophysical Research: Atmospheres, 120, 1536–1564, https://doi.org/10.1002/2014JD022471, 2015.

Xi, X. and Sokolik, I. N.: Quantifying the anthropogenic dust emission from agricultural land use and desiccation of the Aral Sea in Central Asia, Journal of Geophysical Research: Atmospheres, 121, 270–12, https://doi.org/10.1002/2016JD025556, 2016.

Xi, X., Steinfeld, D., Cavallo, S. M., Wang, J., Chen, J., Zulpykharov, K., and Henebry, G. M.: What caused the unseasonal extreme dust storm in Uzbekistan during November 2021?, Environmental Research Letters, 18, 114 029, https://doi.org/10.1088/1748-9326/ad02af, 2023.

https://doi.org/10.5194/egusphere-2025-2808
Preprint. Discussion started: 28 July 2025
© Author(s) 2025. CC BY 4.0 License.

305 Xi, X., Wang, J., Lu, Z., Sayer, A., Lee, J., Levy, R., Wang, Y., Lyapustin, A., Liu, H., Laszlo, I., Ahn, C., Torres, O., Abdullaev, S., Limbacher, J., and Kahn, R.: Analysis of a saline dust storm from the Aralkum Desert - Part 1: Consistency between multisensor satellite aerosol products, Atmospheric Chemistry and Physics, https://doi.org/10.5194/egusphere-2024-3416, 2025.